Magnetic hourglass fermions: From exhaustive symmetry conditions to high-throughput materials predictions

Yating Hu,[1,2] Xiangang Wan,[1] and Feng Tang[1,*]

[1]*National Laboratory of Solid State Microstructures and School of Physics, Nanjing University, Nanjing 210093, China and Collaborative Innovation Center of Advanced Microstructures, Nanjing University, Nanjing 210093, China*

[2]*International Quantum Academy, Shenzhen 518048, China*

(Received 9 June 2022; accepted 7 October 2022; published 26 October 2022)

Many topological band crossings (BCs) have been predicted efficiently utilizing the symmetry properties of wave-functions at high-symmetry points. Among various BCs, the so-called hourglass BCs (with the low-energy excitations dubbed as hourglass fermions) are fascinating since they can be guaranteed to exist under specific symmetry conditions even without realistic calculations. Such novel property renders the theoretical prediction on magnetic topological metals with hourglass BC (which can be Weyl point, Dirac point, lying in nodal loop, and so on) independent on the calculation methods and only determined by the symmetry of crystal and magnetic structure, namely, the magnetic space group (MSG). To date, there have been no magnetic material verified with hourglass fermions. Here we first list all symmetry conditions that allow hourglass BCs in the 1651 MSGs and 528 magnetic layer groups (MLGs) with spin-orbital coupling (SOC): Only 331 MSGs and 53 MLGs can host hourglass BCs. Among these results, the essential hourglass BCs are highlighted, whose MSGs are then applied to predict hundreds of magnetic materials from the MAGNDATA magnetic materials database and first-principles calculations in the frame of LDA + SOC + U verify the hourglass BCs for different values of U. We take $CsMn_2F_6$, synthesized recently with a distorted pyrochlore structure to illustrate the hourglass band structure in detail which is very clear around the Fermi level and the topologically protected surface drumhead states of (100) surface are found to spread over more than one half surface Brillouin zone and only appear in a narrow energy window (∼30 meV), which could induce intriguing stability by prominent electronic correlation. The symmetry-guaranteed existence of hourglass fermion in the predicted magnetic materials is expected to be applied in manipulating band topology by applying appropriate external fields moving the hourglass BC.

DOI: 10.1103/PhysRevB.106.165128

I. INTRODUCTION

The past decade and a half has witnessed the explosive growth of nonmagnetic topological materials (TMs) compared with their magnetic counterparts [1–6], while the verified magnetic counterparts are scarce [7,8], though the first magnetic topological insulator dates from the experimental observation [9] and theoretical interpretation [10] of quantum Hall effect. Nearly one decade ago, through doping the nonmagnetic topological insulator with magnetic ions, quantum anomalous Hall effect was realized [11,12], while the intrinsic magnetic topological materials are very rare and were only theoretically predicted and experimentally verified recently [13–22]. Besides, the classification of band topology in all the 1651 magnetic space groups (MSGs) in the scheme of symmetry-indicator theory [23,24] or topological quantum chemistry [25,26] was obtained, which not only reveals much more diverse topological phases protected by MSG symmetry, and also lay the basis for efficient magnetic topological materials discovery since one only need to calculate the symmetry transformation properties of wave-functions at high-symmetry points [27–30]. Once some constraint arising from the compatibility relations (CRs) on the occurrences of irreducible representations (irreps) at the high-symmetry points is not satisfied, energy bands are thus enforced to cross each other, resulting in various band nodes [31–65]. Interestingly, there exists a very simple-to-use rule for topological materials prediction, both for nonmagnetic and magnetic materials: one might only need to count the electron filling and once the filling is not compatible with a band insulator, band node can thus be guaranteed to appear around the Fermi level [66,67]. As a matter of fact, the filling constraint proves to be very useful and efficient in realistic materials predictions [68,69], especially when the materials calculations might not be very reliable due to electron correlation, leaving the topological character of the enforced band node to be identified through further analysis. As mentioned previously, symmetry information at high-symmetry points can also indicate the existence of band node lying in high-symmetry line/plane connecting the high-symmetry points [23–26,49] due to the breaking of CRs and thus the topological character can be identified [46,56,70,71] when knowing how CRs are broken. However, such identification strongly depends on the representations of wave-functions at high-symmetry points and electron correlation in magnetic materials might reduce the prediction reliability. The first-principles prediction of magnetic topological materials usually depends on the method of

*fengtang@nju.edu.cn

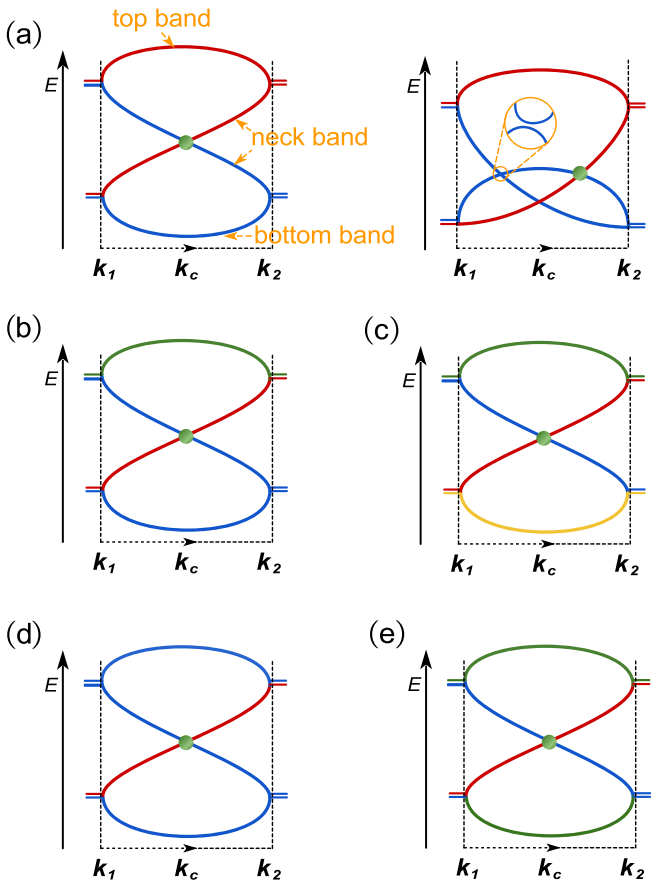

FIG. 1. The hourglass band structures of types A–E are demonstrated in panels (a)–(e), respectively, where the band structures are depicted along $\mathbf{k}_c$ connecting $\mathbf{k}_1$ and $\mathbf{k}_2$. (a) Left panel: the hourglass band structure along $\mathbf{k}_c$ connecting $\mathbf{k}_1$ and $\mathbf{k}_2$. The hourglass BC is denoted by a green dot which is at the crossing point of two neck bands in red and blue. Here different colors denote different (co-)irreps of the little group of $\mathbf{k}_c$. Actually the hourglass band structure here is of type A for the bottom and top bands take the same (co-)irreps as those for the neck bands (our comprehensive study shows that type-A hourglass band structure is the most common one). Right panel: the realistic band structures might be twisted so that the bottom band in panel (a) is put upward to cross the neck bands. Interestingly, the original hourglass BC can be tuned to disappear gradually but a new hourglass BC by green dot is formed. Panels (b)–(e) show the band structures of another four types B–E hourglass. The corresponding splitting patterns are described in the main text. It is easy to find that when we switch the ordering of energy levels at $\mathbf{k}_1$ or $\mathbf{k}_2$, types A–C hourglass BC is stable while the types D and E hourglass BC can be tuned to disappear.

incorporating the electron correlation, which not only affects the ordering of band representations at high-symmetry points, but also even gives a magnetic structure deviating much from the realistic one giving rise to a false MSG.

To find a simple-to-use rule which reveals concrete topological characteristic reliably, in this work we focus on the so-called hourglass band structure [72–76] as shown in Fig. 1: When the (co-)irreps of the energy levels at $\mathbf{k}_1$ and $\mathbf{k}_2$ in the Brillouin zone (BZ) are known, the existence of band node in $\mathbf{k}_c$ which connects $\mathbf{k}_1$ and $\mathbf{k}_2$ is guaranteed. The topological characteristics of such band node can also be identified from the (co-)irreps of the band node [56]. Furthermore, for the hourglass band structure, CRs of the 230 space groups have been applied to obtain an exhaustive list of all hourglass band structures [74], indicating that in many space groups, hourglass band structure exist essentially along some high-symmetry line or plane. This means that for these space groups, we can even not perform first-principles calculations since we already know that the hourglass band structure should exist and the existence should be independent on the calculation details. Furthermore, one can expect that through applying external fields, such as electric or magnetic fields, the (co-)irreps of the energy levels at high-symmetry points retain invariant thus the band node still exists but is only movable flexibly so that large quantum responses could be anticipated [see Fig. 1(a) where the hourglass band structure is twisted by external perturbations, but the hourglass band crossings (BCs) always exist]. Then it is very interesting and also urgently needed to list the hourglass BCs and especially essential ones for all the 1651 MSGs, of which 1421 MSGs describe magnetically ordered materials, which can facilitate realistic magnetic materials predictions with topological BCs and large quantum responses. For magnetic materials, the introduction of new degree of freedom (namely, magnetic ordering) compared to nonmagnetic materials provides the possibility of controlling topological character by tuning magnetic structure [77–80]. In this work, to construct an exhaustive list of all hourglass band structures in all the 1651 MSGs and 528 magnetic layer groups (MLGs), we apply the CRs which are calculated from the (co-)irreps listed in Ref. [47] of all the 1651 MSGs to obtain such list. Since we are interested in electronic materials with nonnegligible spin-orbital coupling (SOC), double-valued representations are used. Besides, for MLGs, we consider some MSGs which allow layer structure once the translation symmetry along some direction is broken. The results for MLGs can be applied to two-dimensional (2D) materials, interfaces or surfaces. In summary, we find that there are 331 MSGs allowing hourglass BCs: 305 MSGs essentially hosting hourglass BCs among which there are 29, 73, 63 and 140 type-I, -II, -III, and -IV MSGs, respectively. We also find that there are 53 MLGs with hourglass BCs which also essentially host hourglass BCs. These MLGs could guide the synthesization of 2D hourglass semimetals and materials discovery combined with first-principles calculations [81]. Once the MSG for a given material is known, we can immediately know the position of hourglass BCs by checking the tabulation in Sec. II of Supplemental Material I [82]. Here for materials searches, we check the magnetic materials as listed in the MAGNDATA database [83,84] whose magnetic structures have already been characterized. We find 175 magnetic materials which are crystallized in 48 of the 305 MSGs with essential hourglass fermions. This indicates that much more hourglass magnetic semimetals are anticipated to exist. We also perform first-principles calculations on these materials to verify the existence of hourglass BCs and select 30 materials with relatively clear hourglass band structures. Furthermore, we also find 13 magnetic materials crystallized in MSGs not in the above 305 ones but hosting hourglass BCs accidentally. These hourglass BCs can be gapped by varying the values of U, the parameter to incorporate the electron

correlation in the first-principle calculations, as demonstrated by our calculations shown in Sec. III of Supplemental Material II [85]. In the following, we first review briefly the strategy of obtaining all symmetry conditions of the formation for hourglass BCs and highlight the essential ones. We then show three magnetic materials examples as predicted to showcase high-quality hourglass band structures near the Fermi level.

II. BRIEF OVERVIEW OF CLASSIFICATION STRATEGY AND ESSENTIAL HOURGLASS BAND STRUCTURE

We first clarify the strategy of exhaustively listing all possible hourglass BCs based on CRs, which was first introduced in Ref. [74] and applied to the 230 space groups with and without time-reversal symmetry, corresponding to type-II and type-I MSGs, respectively. Differently, this work covers all the 1651 MSGs and adopts the convention in Ref. [87]. Concretely, the CRs for all the MSGs are calculated first based on the explicit list of (co-)irreps in Ref. [47]. Note that co-irreps are used when the little group contains antiunitary operation. Related with each hourglass band structure, there is one high-symmetry line or plane ($\mathbf{k}_c$ in Fig. 1) connecting $\mathbf{k}_1$ and $\mathbf{k}_2$, which are high-symmetry points or lie in high-symmetry lines. Note that when $\mathbf{k}_{1/2}$ lies in a high-symmetry line, it represents an arbitrary point in the line, and in this case the infinite points in this line result in infinite hourglass BCs all lying in a nodal line (dubbed as hourglass nodal line). For each of $\mathbf{k}_1$ and $\mathbf{k}_2$, there are two energy levels participating in the formation of hourglass band structure which would split along $\mathbf{k}_c$. The band splitting pattern is encoded in the CRs. For later clarification, we name the highest energy band of the hourglass band structure as "top band," the lowest energy band as "bottom band", and the remaining two bands in the middle part as "neck bands," as shown in Fig. 1(a). To ensure that the hourglass BC is stable, $\mathbf{k}_c$ should allow at least two different (co-)irreps and the hourglass BC is formed by the crossing of the neck bands carrying different (co-)irreps of X. Then, we can classify the hourglass band structures into five types: The bottom and top bands own different (co-)irreps and these (co-)irreps are simply those of the neck bands [type A, see Fig. 1(a)], or only share one (co-)irrep with those of the neck bands [type B, see Fig. 1(b)] and share no (co-)irreps with those of then neck bands [type C, see Fig. 1(c)]; The bottom and top bands own the same (co-)irrep and it take one of the (co-)irreps of the neck bands [type D, see Fig. 1(d)] or take a different (co-)irrep from those of the neck bands [type E, see Fig. 1(e)]. For all the five types, it is easy to find that the formation of the hourglass BC is due to the interchange of the two (co)-irreps in the hourglass BC from $\mathbf{k}_1$ to $\mathbf{k}_2$ through $\mathbf{k}_c$. We list all possible hourglass band structures in Sec. II of Supplemental Material I [82], for each of which we provide the coordinates of k in the trio $\mathbf{k}_1 - \mathbf{k}_c - \mathbf{k}_2$ following the convention in Ref. [87] and the related CRs.

With respect to MSGs or MLGs hosting essential hourglass BC, namely, the hourglass BC definitely exists as long as the material is crystallized in the MSG or MLG, we only need to focus on types A–C hourglass band structure, since type-D and -E hourglass band structures can be tuned to disappear by changing the ordering of energy levels at $\mathbf{k}_1$ or $\mathbf{k}_2$. For the types A–C hourglass band structures to be essential, it should be required that, all CRs from $\mathbf{k}_1$ (and $\mathbf{k}_2$) to $\mathbf{k}_c$ should be in the form of $D(\mathbf{k}_{1,2})^{i_{1,2}} \longrightarrow D(\mathbf{k}_c)^{j_{1,2}} \oplus D(\mathbf{k}_c)^{j'_{1,2}}$ where $i_{1,2}$ and $j_{1,2}(j'_{1,2})$ denote the (co-)irrep of little group of $\mathbf{k}_{1,2}$ and $\mathbf{k}_c$, respectively (note that $j_{1,2}$ might be equal to $j'_{1,2}$). Besides, $\{D(\mathbf{k}_c)^{j_1}, D(\mathbf{k}_c)^{j'_1}\}$ cannot be equal to $\{D(\mathbf{k}_c)^{j_2}, D(\mathbf{k}_c)^{j'_2}\}$ otherwise the bands carrying these (co-)irreps can be connected and gapped from other band structures within $\mathbf{k}_c$, which is obviously not an hourglass band structure. Imposing the above requirements on essential hourglass band structures, we thus obtain all essential hourglass band structures, and as long as the MSG or MLG allows essential hourglass band structure along some high-symmetry line or plane, this MSG or MLG is listed in Table I. For the essential hourglass band structures, the types (namely, types A, B, and C) are printed in red in Sec. II of Supplemental Material I [82]. The results of MSGs listed in Table I provide a powerful guide of searching for (nearly) ideal magnetic hourglass metals: As long as the material is crystallized in any MSG in Table I, the hourglass BC definitely exists and thus could appear near the Fermi level easily.

III. MATERIALS INVESTIGATION

The list of all possible symmetry conditions of hourglass band structures could aid in materials predictions and design. Compared with the studies of nonmagnetic topological materials, those for the magnetic counterparts have achieved much less progress. Recently, the magnetic topological quantum chemistry has been applied to high-throughput calculations of magnetic topological materials [30], which enlarge the candidates of magnetic topological materials, showcasing that the utilization of symmetry information can make the prediction of magnetic topological materials more efficient and especially, more reliable. However, the topological characters of the predicted symmetry-enforced magnetic topological semimetals remain unclear and the BC formed by band inversion could disappear choosing different values of U. With respect to the hourglass band structure here, we aim at predicting many magnetic materials hosting hourglass BCs around the Fermi level. Hence, we only need to match the MSGs of the magnetic materials candidates with the 305 ones listed in Table I, and due to that the hourglass band structures definitely exist along some k path in these MSGs, the hourglass fermions should tend to appear very close to the Fermi level. In total, we find 175 stoichiometric magnetic materials essentially hosting hourglass fermions as listed in the MAGNDATA database [83,84], belonging to 48 of the 305 MSGs. We note that the MAGNDATA database [83,84] contains only 335 MSGs in total, indicating that more magnetic materials should be synthesized in future and thus more hourglass magnetic materials could be found. For these materials, all materials allow the existence of type-A hourglass band structures and only 16 materials can host type-C hourglass ones. Out of these materials, we highlight 30 which are found to demonstrate relatively clear hourglass band structure near the Fermi level for reasonable values of U from LDA + SOC + U calculations [88], as listed in Table III alongside with the statistics of materials with collinear and noncollinear magnetic structures for type-I, -III, and -IV MSGs. Besides, we note that the degeneracy of the hourglass BC can only be 2 and 4 and most hourglass BCs

TABLE I. All MSGs and MLGs hosting essential hourglass BCs: The first column denotes the types of the MSGs and the second column contains the names of MSGs or MLGs in the Belov-Neronova-Smirnova [86] notation. Note that when the MSG name is printed in bold, it means that the MSG can also allow an MLG hosting essential hourglass BC when the translation symmetry along some direction is broken and such direction is given in the parentheses. There are in total 305 MSGs and 53 MLGs with essential hourglass BCs. Of 305 MSGs, 288 can host type-A hourglass BCs and 94 can host type-C hourglass BCs. For MLGs, 51 and 10 can host type-A and type-C hourglass BCs, respectively. The MSGs 62.446 and 62.447 are printed in red, to which three magnetic materials are taken as examples to demonstrate hourglass BCs in the main text.

	MSG (MLG)
I	48.257; **50.277 (c)**; 52.305; **54.337 (b)**; 56.365; **57.377 (c)**; **59.405 (c)**; 60.417; 61.433; 62.441; 68.511; 70.527; 93.119; 94.127; 98.157; 125.363; 126.375; 130.423; 132.447; 133.459; 134.471; 137.507; 141.551; 142.561; 201.18; 203.26; 205.33; 222.98; 230.145;
II	**4.8 (a,b)**; **7.25 (a,c)**; 9.38; **17.8 (a,b)**; **18.17 (c)**; 19.26; 20.32; **26.67 (a)**; **28.88 (a,c)**; **29.100 (a)**; **30.112 (a)**; **31.124 (a)**; **32.136 (c)**; 33.145; 34.157; 36.173; **39.196 (c)**; 40.204; 41.212; 43.225; 45.236; 46.242; 52.306; **54.338 (b)**; 56.366; **57.378 (c)**; 60.418; 61.434; 62.442; 76.8; 77.14; 78.20; 80.30; **90.96 (c)**; 91.104; 92.112; 93.120; 94.128; 95.136; 96.144; 98.158; **100.172 (c)**; 102.188; 104.204; 106.220; 108.234; 109.240; 110.246; **113.268 (c)**; 114.276; **117.300 (c)**; 118.308; 120.322; 122.334; 130.424; 133.460; 138.520; 158.58; 159.62; 161.70; 169.114; 170.118; 173.130; 178.156; 179.162; 182.180; 185.198; 186.204; 188.216; 190.228; 205.34; 219.86; 220.90;
III	**29.101 (a)**; **29.103 (a)**; 33.146; 33.148; 52.310; 52.311; 52.312; **54.342 (b)**; 54.343; **54.344 (b)**; 56.369; 56.370; **57.382 (c)**; **57.383 (c)**; 57.384; 60.422; 60.423; 60.424; 61.436; 62.446; 62.447; 62.448; 73.551; **85.61 (c)**; 86.69; 88.83; 106.223; 110.247; 110.249; 120.323; 124.355; **125.367 (c)**; 126.378; 126.379; **127.390 (c)**; 128.402; **129.415 (c)**; 130.426; 130.427; 130.429; 133.462; 133.463; 133.465; 133.467; 134.475; 135.486; 135.489; 135.491; 136.498; 137.510; 137.511; 138.522; 138.523; 138.525; 141.554; 142.564; 142.567; 219.87; 222.101; 224.113; 226.125; 227.131; 228.137;
IV	**4.10 (b)**; **7.27 (c)**; **7.29 (a)**; 7.30; 9.41; **17.11 (a)**; 17.14; **18.20 (c)**; 18.21; 18.22; 19.28; 19.29; 20.36; **25.61 (a,b)**; **25.64 (a)**; 25.65; 26.71; **26.72 (a)**; 26.76; 27.85; 27.86; **28.92 (c)**; **28.94 (a)**; **28.95 (a)**; 28.96; 28.98; 29.104; **29.105 (a)**; **29.106 (a)**; **29.107 (a)**; 29.108; 29.109; 29.110; 30.116; **30.118 (a)**; 30.120; 30.121; 30.122; 31.128; 31.129; **31.130 (a)**; 31.132; 31.133; 32.139; **32.140 (c)**; 32.142; 32.143; 33.149; 33.150; 33.151; 33.152; 33.153; 33.154; 33.155; 34.160; 34.161; 34.162; 35.169; 35.171; 36.178; 38.194; 39.201; 40.208; 41.216; 41.217; 43.228; 44.233; 45.240; 46.247; 50.286; 50.288; 52.315; 54.347; 54.351; 54.352; 56.372; 57.388; 57.389; 59.413; 59.414; 60.426; 60.428; 60.429; 61.438; 62.452; 62.455; 77.16; 77.17; 77.18; 80.32; 90.100; 92.116; 93.124; 93.125; 93.126; 94.132; 94.133; 94.134; 96.148; 98.162; 99.168; 99.170; 100.175; 100.178; 101.184; 102.192; 102.194; 103.202; 104.208; 105.216; 101.186; 105.217; 105.218; 106.224; 106.226; 109.244; 110.250; 111.256; 111.258; 113.272; 113.274; 114.280; 115.288; 115.290; 116.298; 117.304; 117.306; 118.312; 119.320; 122.338; 125.374; 132.458; 133.470; 134.480; 137.516; 137.517; 138.530; 183.190; 215.73; 216.77;

are twofold degenerate. We list in Table II all MSGs/MLGs allowing fourfold degenerate hourglass BCs alongside with the predicted magnetic materials. In the following, we showcase the hourglass band structures and detailed analysis on the topological characteristics of the hourglass BCs in magnetic materials $CsMn_2F_6$ [89], NdSi [90–92] and MnCoGe [93–95]. Other than these three materials demonstrated in the main text, all the band structures of the calculated 175 magnetic hourglass materials are provided in Sec. IV of Supplemental Material II [85].

A. Material example: $CsMn_2F_6$

$CsMn_2F_6$, a recently synthesized materials with distorted pyrochlore structure, exhibits a transition to a long-range ordered magnetic state at a temperature of 24.1 K [89]. It is crystallized in MSG 62.447 of type III, with orthorhombic lattice, whose BZ is shown in Fig. 2(b). The unitary point group is D_{2h} whose the main axis is along x axis but there exists antiunitary point symmetry (namely, combination of time-reversal, $\mathcal{T}$ and spatial operation), which can be chosen

TABLE II. All MSGs and MLGs hosting fourfold degenerate hourglass BCs. We list six materials from the MAGNDATA database crystallized in any of the MSGs in the table. The magnetic material is identified by its chemical formula, its MSG and the entry (in parentheses) in the MAGNDATA database, and separated by comma. For example, "IV, 54.352: $BaCo_2V_2O_8$ (1.30)" characterizes one magnetic material whose chemical formula is $BaCo_2V_2O_8$. Its MSG is 54.352 of type IV and its entry in the MAGNDATA database is 1.30.

		MSG(MLG)
II		50.306; 52.315; 54.338 (b); 57.378 (c); 60.418; 61.434; 62.442; 106.220; 130.424; 130.426; 133.460; 205.34; 222.99; 226.123; 228.135;
III		133.467; 135.491; 222.102;
IV		50.286; 50.288; 54.347; 54.351; 54.352; 59.414; 60.426; 60.428; 60.429; 61.438; 62.452; 62.455; 101.186; 102.192; 105.217; 125.374; 132.458; 133.470; 134.480; 137.516; 137.517; 138.530; 221.97;
	Materials	IV, 54.352 : $BaCo_2V_2O_8$(1.30); IV, 54.352 : Sr_2IrO_4(1.3); IV, 54.352 : Sr_2IrO_4(1.77); IV, 62.452 : IV Mn_3O_4 (1.1); IV, 62.452 : VPO_4 (1.523); IV, 62.452 : $TbGe_3$ (2.36);

TABLE III. Classification of 175 stoichiometric magnetic materials based on magnetic structure (parallel or antiparallel and collinear) and selected magnetic materials with relatively clear hourglass band structure. The magnetic material is identified by its chemical formula, its MSG and the entry (in parentheses) in the MAGNDATA database, and separated by comma. For example, "III, 62.446: MnCoGe (0.445)" characterizes one magnetic material whose chemical formula is MnCoGe. Its MSG is 62.446 of type III and its entry in the MAGNDATA database is 0.445.

Magnetic Ordering		I	III	IV	Total	Selected Materials
Collinear	Parallel	0	6	0	6	III, 62.446 : $MnCoGe$ (0.445), $SrRuO_3$ (0.732); III, 62.448 : Tb_3NiGe_2 (0.439);
	Anti-Parallel	10	30	45	85	IV, 7.29 : Na_2MnF_5 (1.55); III, 33.146 : Fe_2O_3 (0.299, 0.300), $GaFeO_3$ (0.38); I, 61.433 : Ca_2RuO_4 (0.398), $MnSe_2$ (1.0.47); I, 62.441 : $CuFePO_5$ (0.260), $NiFePO_5$ (0.261), Fe_2PO_5 (0.263); III, 62.448 : $NaOsO_3$ (0.25), $YRuO_3$ (0.513); III, 125.367 : $CeMn_2Ge_4O_{12}$ (0.189), $ZrMn_2Ge_4O_{12}$ (0.315);
Non-Collinear		17	44	23	84	I, 62.441 : Mn_2GeO_4 (0.102), Co_2SiO_4 (0.218, 0.219), $CoSO_4$(0.571, 0.96); III, 62.446 : $TeNiO_3$ (0.94), $NdSi$ (0.407); III, 62.447 : $CoFePO_5$ (0.262), $CsMn_2F_6$ (0.726); III, 62.448 : $LaMnO_3$ (0.1); I, 205.33 : $MnTe_2$ (0.20); III, 224.113 : USb (3.12), UO_2 (3.2), $NpBi$ (3.7);
Total		27	80	68	175	30

as $c_{2z}\mathcal{T}$, twofold rotation around z axis (thus $c_{2z}\mathcal{T}\cdot D_{2h}$ contains all antiunitary point symmetries). The crystal structure of this material is shown in Fig. 2(a) where it can be found that Mn ions are located at the center of the octahedron of F ions. These octahedra are connected at the corner. As shown in Fig. 2(a), the magnetic moments of Mn ions own very small canting angles between each other while they are almost locked with the corresponding octahedra, indicative of significant SOC. The electronic band structure is shown in Fig. 3(a) with U set to be 3 eV. As listed in Sec. II of Supplemental Material I [82], for MSG 62.447, there are high-symmetry line D and high-symmetry plane $P5$ which can host hourglass band structures (see pages 304–306 of Supplemental Material I), both of which can host type-A essential hourglass band structures. The coordinates of them are $(-w, \frac{1}{2}, 0)$ and $(u, \frac{1}{2}, v)$ in the convention adopted in Ref. [87] (namely, in the basis of reciprocal basis lattice vectors dual to the primitive lattice basis vectors), respectively, which are $(\frac{\pi}{a}, w, 0)$ and $(\frac{\pi}{a}, u, v)$ after transformed to the Cartesian coordinates, corresponding to XS and UXS as shown in Fig. 2(b), respectively. Written in the trio form of $\mathbf{k}_1 - \mathbf{k}_c - \mathbf{k}_2$, here we have $S{-}D{-}X$, $S{-}P5{-}X$, $X{-}P5{-}Q$, $S{-}P5{-}U$, $Q{-}P5{-}U$, $P{-}P5{-}S$, $G{-}P5{-}S$, $Q{-}P5{-}P$ and $G{-}P5{-}Q$, where S, X and U are high-symmetry points whose Cartesian coordinates are $(\frac{\pi}{a}, \frac{\pi}{b}, 0)$, $(\frac{\pi}{a}, 0, 0)$ and $(\frac{\pi}{a}, 0, \frac{\pi}{c})$, respectively and Q, P and G are high-symmetry lines whose Cartesian coordinates are $(\frac{\pi}{a}, \frac{\pi}{b}, w)$, $(\frac{\pi}{a}, w, \frac{\pi}{b})$ and $(\frac{\pi}{a}, 0, w)$, respectively. Take $S-D-X$ as an example. S owns two co-irreps denoted by $\{1,3\}$ and $\{2,4\}$, which would split into $\{1\}\oplus\{1\}$ and $\{2\}\oplus\{2\}$ in D by CRs also shown in Sec. II of Supplemental Material I, and X can only allow one co-irrep denoted by $\{1\}$ which splits into $\{1\}\oplus\{2\}$ in D. The CRs would thus require that hourglass BC essentially appear in D. The hourglass band structures of the material for all the trios shown above can be easily found in Fig. 3(a). Furthermore, it is easy to know that these hourglass BCs are doubly-fold-degenerate since the two co-irreps of D are both of dimension being 1.

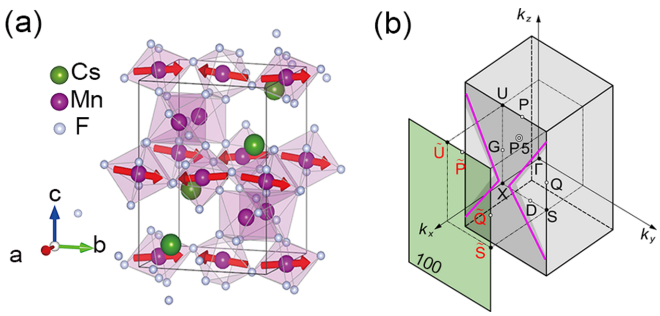

FIG. 2. (a) The crystal and magnetic structure of $CsMn_2F_6$ crystallized in MSG 62.447. (b) The BZ of MSG 62.447 and the (100) surface BZ.

According to the CRs-required band splitting around any band node in Ref. [56], we can know that the hourglass BC in D actually lies in a nodal line within the high-symmetry plane $P5$. This is consistent with that $P5$ can also host hourglass BC, which definitely lies in a nodal line within $P5$. The essential existence of hourglass BCs in the above trios enforces the shape of nodal line within $P5$. As shown in Fig. 3(e), the two energy branches in orange and green touch each other to form a nodal line, and through MSG symmetries, there should exist four nodal line segments demonstrated in Fig. 2(b) by the pink lines. Note that the energy zone for this nodal line is very narrow and thus constitutes a nearly ideal line-like Fermi surface. By Ref. [56] which lists all $k\cdot p$ models around all band nodes, we quickly know that around each point in this nodal line, the low-energy $k\cdot p$ model is $(R_2q_y + R_1q_z)\sigma_0 + R_3q_x\sigma_1 + R_4q_x\sigma_2 + (R_6q_y + R_5q_z)\sigma_3$ where σ_0 is identity matrix, $\sigma_{x/y/z}$ is Pauli matrix, (q_x, q_y, q_z) is the momentum measured from the point and R_is are all real parameters. The nodal line is further found to possess π Berry phase. Hence, drumhead surface states [39] are anticipated as shown in Figs. 3(f) and 3(g) and spread the shadow area in Fig. 2(b). The evolution of the energy contours for (100) surface states with different energies can be found in Movie, by which the drumhead states are observed to be restricted in a very narrow energy window of around 30 meV. Hence, such flat surface states can undergo stability toward exotic ordering phase such as superconducting state by interactions [39]. Note that the hourglass BCs here emerging within the unoccupied/occupied bands, could also lead to surface states

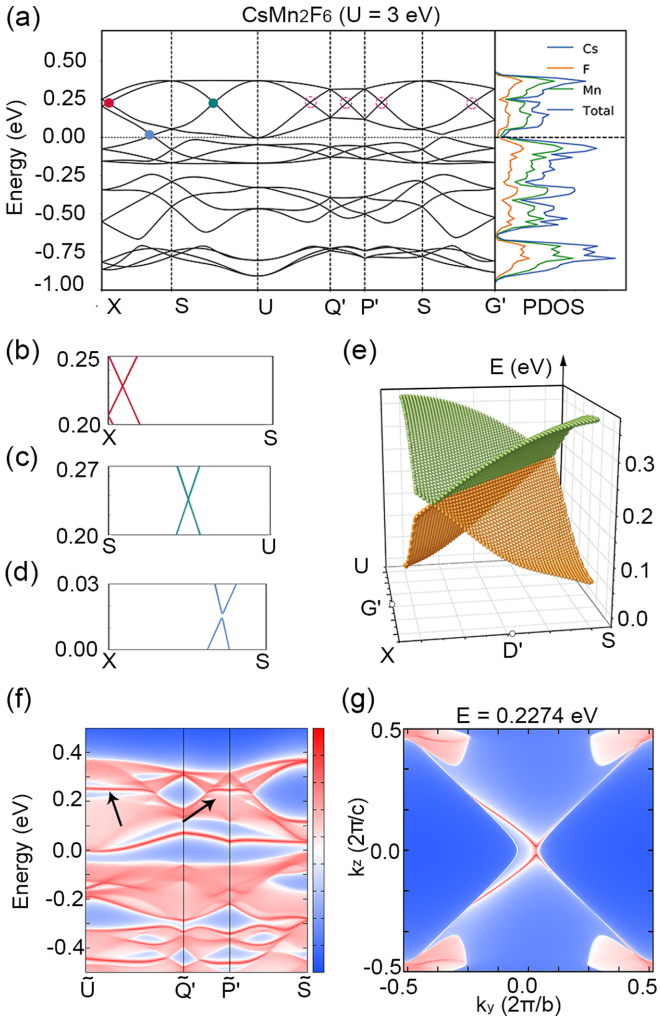

FIG. 3. (a) The electronic band structure of $CsMn_2F_6$ and the plot of density of states (with $U=$ 3 eV). Q', P', G' represents a middle point located on path C, D, G. The hourglass shapes are found to be very clear and also close to the Fermi level. Note that there is a tiny gap within the blue circle as shown in (d), which is consistent with the fact that the two bands in the blue circle are found to own the same co-irrep so that the hybridization between them is not prohibited. In the energy window (−0.7 eV,0.5 eV), we can easily find many clear hourglass band structures along different k paths. We take two hourglass BCs as indicated by the red and green circles as examples and the enlarged band plots are shown in (b) and (c), respectively. (e) The 3D band plot with respect to the $k_x = \frac{\pi}{a}$ plane, namely, the plane UXS shown in Fig. 2(b). The hourglass BCs shown in (a) with energy around 0.25 eV are all located in the nodal line in this plane, formed by the touching of two green and orange energy curves. The projection of the nodal line is shown by pink lines in Fig. 2(b). Panels (f) and (g) contain the results for surface states indicated by the red color: The black arrow in panel (f) denotes the associated surface states while panel (g) is the energy contour at 0.2274 eV for surface states. Note that the c_{2x} symmetry is broken in the slab used to calculate the surface states while $c_{2z}T$ symmetry is still preserved. The drumhead surface states are found to spread over most of the surface BZ as shown by shadow area in Fig. 2(b), and their energies are restricted to a very narrow region (∼30 meV).

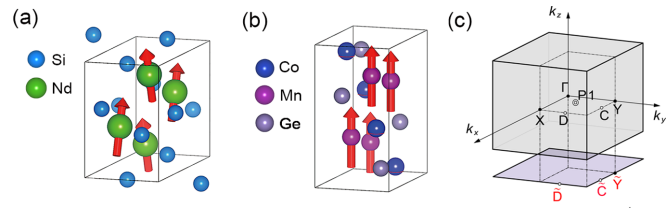

FIG. 4. The crystal and magnetic structures of NdSi (a) and MnCoGe (b). They are both crystallized in MSG 62.446 whose BZ is shown in panel (c) as well as the (001) surface BZ.

as verified by our calculations. These hourglass excitations are not far from the Fermi level, and might be accessed by slightly doping. Furthermore, even the hourglass BCs (though predicted to always exist by symmetry) are found relatively far from the Fermi level, some fascinating transport behaviors could still be experimentally observed, as exemplified by the type-II Dirac points located around 0.55 eV, 0.8 eV, and 1 eV below the Fermi level in $PdTe_2$ [96,97], $PtTe_2$ [98], and $PtSe_2$ [99], respectively. The interplay of magnetic order, nontrivial bulk topology, relatively clean Fermi surface and nearly perfect hourglass nodal line and exotic surface states make this material so attractive that it is expected to be verified in future experimental studies.

B. Material example: NdSi and MnCoGe

Then we discuss materials NdSi and MnCoGe, whose ground states have been confirmed to be ferromagnetic with Curie temperatures $T_c \sim$ 46 K and 345 K, respectively, by neutron diffraction experiments [90–95]. They are both crystallized in MSG 62.446, also of type III from Table I, with orthorhombic lattice. The crystal structures of NdSi and MnCoGe are shown in Figs. 4(a) and 4(b), and the corresponding BZ is shown in Fig. 4(c). The point group is also D_{2h} but the corresponding main axis is along z axis. For MSG 62.446, the antiunitary point symmetry can be chosen as $c_{2x}T$, the symmetry of all k points in $P5$. Noting that c_{2x} of this MSG corresponds to a screw symmetry actually, we then find each energy level in $P5$ should own a Kramer's degeneracy and furthermore we find that there is only one co-irrep for $P5$, thus $P5$ cannot allow hourglass band structure in this MSG, different from the above MSG. Actually, from Sec. II of Supplemental Material I [82], we find that only the high-symmetry plane $P1(u, v, 0)$ can host essential type-A hourglass BC which is further identified to lie in a nodal line within this high-symmetry plane. The related trios are found to be $X-P1-Y$, $Y-P1-D$, $X-P1-C$, $D-P1-C$, where X and Y are two high-symmetry points whose Cartesian coordinates are $(\frac{\pi}{a}, 0, 0)$ and $(0, \frac{\pi}{b}, 0)$ and C and D are two high-symmetry lines whose Cartesian coordinates are $(w, \frac{\pi}{b}, 0)$ and $(\frac{\pi}{a}, w, 0)$, respectively. The electronic band structures for NdSi with $U = 4$ eV and MnCoGe with $U =$ 0 eV are shown in Figs. 5(a) and 5(c), demonstrating clear hourglass band structures as expected. The associated surface states are shown in Figs. 5(b) and 5(d).

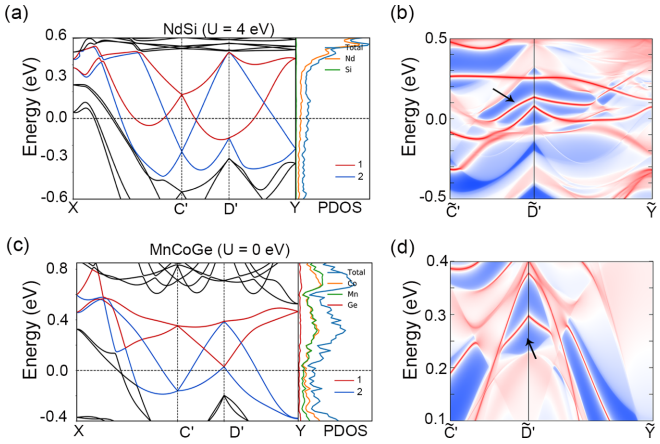

FIG. 5. The results for NdSi (a, b) and MnCoGe (c, d). Panels (a) and (c) correspond to the electronic band structures of NdSi and MnCoGe, respectively (as well as the plots of density of states) from which the hourglass band structures can be clearly identified (1 and 2 represent two different irreps). For both materials, U is respectively chosen to be 4 eV and 0 eV. C', D' represents a point on path C, D. The hourglass BCs actually lie in a nodal line with π Berry phase, the associated surface states for (001) surface are calculated and shown in panels (b) and (d), where drumhead states can be expected, indicated by black arrow.

IV. CONCLUSIONS AND PERSPECTIVES

To conclude, we first obtained all possible hourglass fermions realized in 3D/2D magnetic/nonmagnetic materials purely based on symmetry arguments: Using the double-valued irreps or co-irreps of little groups of k points in the BZ and their CRs which encode the band splitting patterns, we list all concrete positions and related CRs of hourglass BCs in Supplemental Material I [82]. In total, 331 MSGs and 53 MLGs allow existence of hourglass BCs. Furthermore, we highlight 305 MSGs essentially with hourglass BCs since any materials crystallized in any of these MSGs definitely host hourglass fermions around the Fermi level (All the 53 MLGs essentially host hourglass BCs); 232 of these 305 MSGs describe the symmetry of magnetically ordered materials and are around five times the number (48) of MSGs in the MAGNDATA database [83,84]. Then we performed high-throughput calculations based on the MSGs which essentially host hourglass BCs and demonstrate the hourglass BCs in 175 realistic magnetic materials in the MAGNDATA database [83,84]. The prediction of hourglass BCs in these magnetic materials is reliable since the MSGs of these materials, related with their magnetic structures, are characterized precisely [83,84]. The magnetic structures of more magnetic materials could be characterized by advanced neutron scattering techniques, for which whether they can host hourglass fermions can be known simply by checking our tabulation. We also expect the results of symmetry conditions could be applied in predicting more magnetic systems, such as 2D hourglass magnetic material and magnetic Hopf-link semimetals, as well as coexisting hourglass BCs with other exotic ordering such as ferroelectricity and superconductivity. The plethora of materials predictions in this work could attract further theoretical and experimental studies in future. Finally, we expect that the MSGs/MLGs with hourglass BCs could also be utilized to inversely determine the magnetic structures of magnetic materials.

V. METHOD

The first-principles calculations, incorporating SOC for all 175 stoichiometric magnetic materials, are implemented in the Vienna *ab initio* simulation package (VASP). The LDA + U scheme [88] was employed for these materials with different Hubbard U parameters: coulomb interaction $U = 0, 1, 2, 3, 4$ eV on magnetic moments of the magnetic materials with $3d/4d$ electrons, while $U = 0, 2, 4, 6$ eV for $4f/5f$ electron (refer to Sec. II of Supplemental Material II [85] for further details). The energy cutoff was set to 500 eV and a k mesh of $0.06\pi/$Å k-space resolution was adopted to sample the BZ. The convergence criterion for the total energy was set to be 10^{-5}eV. Other than calculated magnetic moments on each nonequivalent magnetic atoms, we display their energy band structures through specific high-symmetry path where hourglass fermion lies based on our symmetry analysis results in Sec. II of Supplemental Material I [82]. The surface states are performed on $CsMn_2F_6$, NdSi and MnCoGe by WANNIER90 code [100,101] as a post processing step of the first-principles calculations. We take a disentangle calculation to construct an effective tight-binding Hamiltonian on the basis of the maximally localized Wannier function based on first-principles calculations, the method developed by Marzari and co-workers [102,103].

ACKNOWLEDGMENTS

F.T. was supported by National Natural Science Foundation of China (NSFC) under Grant No. 12104215 and Young Elite Scientists Sponsorship Program by China Association for Science and Technology. Y.H., F.T., and X.W. were supported by the National Key R&D Program of China (Grant No. 2018YFA0305704), NSFC Grants No. 12188101, No. 11834006, No. 51721001, and No. 11790311, and the excellent program at Nanjing University. X.W. also acknowledges the support from the Tencent Foundation through the XPLORER PRIZE.

[1] M. Z. Hasan and C. L. Kane, Colloquium: Topological insulators, Rev. Mod. Phys. **82**, 3045 (2010).

[2] X. L. Qi and S. C. Zhang, Topological insulators and superconductors, Rev. Mod. Phys. **83**, 1057 (2011).

[3] A. Bansil, H. Lin, and T. Das, Colloquium: Topological band theory, Rev. Mod. Phys. **88**, 021004 (2016).

[4] Y. Ando and L. Fu, Topological crystalline insulators and topological superconductors: From concepts to materials, Annu. Rev. Condens. Matter Phys. **6**, 361 (2015).

[5] N. P. Armitage, E. J. Mele, and A. Vishwanath, Weyl and Dirac semimetals in three-dimensional solids, Rev. Mod. Phys. **90**, 015001 (2018).
[6] T. O. Wehling, A. M. Black-Schaffer, and A. V. Balatsky, Dirac materials, Adv. Phys. **63**, 1 (2014).
[7] Y. Tokura, K. Yasuda, and A. Tsukazaki, Magnetic topological insulators, Nat. Rev. Phys. **1**, 126 (2019).
[8] B. A. Bernevig, C. Felser, and H. Beidenkopf, Progress and prospects in magnetic topological materials, Nature (London) **603**, 41 (2022).
[9] K. v. Klitzing, G. Dorda, and M. Pepper, New Method for High-Accuracy Determination of the Fine-Structure Constant Based on Quantized Hall Resistance, Phys. Rev. Lett. **45**, 494 (1980).
[10] D. J. Thouless, M. Kohmoto, M. P. Nightingale, and M. den Nijs, Quantized Hall Conductance in a Two-Dimensional Periodic Potential, Phys. Rev. Lett. **49**, 405 (1982).
[11] R. Yu, W. Zhang, H. J. Zhang, S. C. Zhang, X. Dai, and Z. Fang, Quantized anomalous Hall effect in magnetic topological insulators, Science **329**, 61 (2010).
[12] C. Z. Chang, J. Zhang, X. Feng, J. Shen, Z. Zhang, M. Guo, K. Li, Y. Ou, P. Wei, L. L. Wang, Z. Q. Ji, Y. Feng, S. Ji, X. Chen, J. Jia, X. Dai, Z. Fang, S. C. Zhang, K. He, Y. Wang *et al.*, Experimental observation of the quantum anomalous Hall effect in a magnetic topological insulator, Science **340**, 167 (2013).
[13] Y. Gong, J. Guo, J. Li, K. Zhu, M. Liao, X. Liu, Q. Zhang, L. Gu, L. Tang, X. Feng, D. Zhang, W. Li, C. Song, L. Wang, P. Yu, X. Chen, Y. Wang, H. Yao, W. Duan, Y. Xu *et al.*, Experimental realization of an intrinsic magnetic topological insulator, Chin. Phys. Lett. **36**, 076801 (2019).
[14] J. Li, Y. Li, S. Du, Z. Wang, B. L. Gu, S. C. Zhang, K. He, W. Duan, and Y. Xu, Intrinsic magnetic topological insulators in van der Waals layered $MnBi_2$ Te_4-family materials, Sci. Adv. **5**, eaaw5685 (2019).
[15] D. Zhang, M. Shi, T. Zhu, D. Xing, H. Zhang, and J. Wang, Topological Axion States in the Magnetic Insulator $MnBi_2Te_4$ with the Quantized Magnetoelectric Effect, Phys. Rev. Lett. **122**, 206401 (2019).
[16] C. Liu, Y. Wang, H. Li, Y. Wu, Y. Li, J. Li, K. He, Y. Xu, J. Zhang, and Y. Wang, Robust axion insulator and Chern insulator phases in a two-dimensional antiferromagnetic topological insulator, Nat. Mater. **19**, 522 (2020).
[17] M. M. Otrokov, I. I. Klimovskikh, H. Bentmann, D. Estyunin, A. Zeugner, Z. S. Aliev, S. Gaß, A. U. B. Wolter, A. V. Koroleva, A. M. Shikin, M. Blanco-Rey, M. Hoffmann, I. P. Rusinov, A. Y. Vyazovskaya, S. V. Eremeev, Y. M. Koroteev, V. M. Kuznetsov, F. Freyse, J. Sánchez-Barriga, I. R. Amiraslanov *et al.*, Prediction and observation of an antiferromagnetic topological insulator, Nature (London) **576**, 416 (2019).
[18] Y. Deng, Y. Yu, M. Z. Shi, Z. Guo, Z. Xu, J. Wang, X. H. Chen, and Y. Zhang, Quantum anomalous Hall effect in intrinsic magnetic topological insulator $MnBi_2$ Te_4, Science **367**, 895 (2020).
[19] E. Liu, Y. Sun, N. Kumar, L. Muechler, A. Sun, L. Jiao, S. Y. Yang, D. Liu, A. Liang, Q. Xu, J. Kroder, V. Süß, H. Borrmann, C. Shekhar, Z. Wang, C. Xi, W. Wang, W. Schnelle, S. Wirth, Y. Chen *et al.*, Giant anomalous Hall effect in a ferromagnetic kagome-lattice semimetal, Nat. Phys. **14**, 1125 (2018).
[20] N. Morali, R. Batabyal, P. K. Nag, E. Liu, Q. Xu, Y. Sun, B. Yan, C. Felser, N. Avraham, and H. Beidenkopf, Fermi-arc diversity on surface terminations of the magnetic Weyl semimetal $Co_3Sn_2S_2$, Science **365**, 1286 (2019).
[21] D. F. Liu, A. J. Liang, E. K. Liu, Q. N. Xu, Y. W. Li, C. Chen, D. Pei, W. J. Shi, S. K. Mo, P. Dudin, T. Kim, C. Cacho, G. Li, Y. Sun, L. X. Yang, Z. K. Liu, S. S. P. Parkin, C. Felser, and Y. L. Chen, Magnetic Weyl semimetal phase in a Kagome crystal, Science **365**, 1282 (2019).
[22] I. Belopolski, K. Manna, D. S. Sanchez, G. Chang, B. Ernst, J. Yin, S. S. Zhang, T. Cochran, N. Shumiya, H. Zheng, B. Singh, G. Bian, D. Multer, M. Litskevich, X. Zhou, S. M. Huang, B. Wang, T. R. Chang, S. Y. Xu, A. Bansil *et al.*, Discovery of topological Weyl fermion lines and drumhead surface states in a room temperature magnet, Science **365**, 1278 (2019).
[23] H. C. Po, A. Vishwanath, and H. Watanabe, Complete theory of symmetry-based indicators of band topology, Nat. Commun. **8**, 1 (2017).
[24] H. Watanabe, H. C. Po, and A. Vishwanath, Structure and topology of band structures in the 1651 magnetic space groups, Sci. Adv. **4**, eaat8685 (2018).
[25] B. Bradlyn, L. Elcoro, J. Cano, M. G. Vergniory, Z. Wang, C. Felser, M. I. Aroyo, and B. A. Bernevig, Topological quantum chemistry, Nature (London) **547**, 298 (2017).
[26] L. Elcoro, B. J. Wieder, Z. Song, Y. Xu, B. Bradlyn, and B. A. Bernevig, Magnetic topological quantum chemistry, Nat. Commun. **12**, 4 (2021).
[27] T. Zhang, Y. Jiang, Z. Song, H. Huang, Y. He, Z. Fang, H. Weng, and C. Fang, Catalogue of topological electronic materials, Nature (London) **566**, 475 (2019).
[28] M. G. Vergniory, L. Elcoro, C. Felser, N. Regnault, B. A. Bernevig, and Z. Wang, A complete catalogue of high-quality topological materials, Nature (London) **566**, 480 (2019).
[29] F. Tang, H. C. Po, A. Vishwanath, and X. Wan, Comprehensive search for topological materials using symmetry indicators, Nature (London) **566**, 486 (2019).
[30] Y. Xu, L. Elcoro, Z. D. Song, B. J. Wieder, M. G. Vergniory, N. Regnault, Y. Chen, C. Felser, and B. A. Bernevig, High-throughput calculations of magnetic topological materials, Nature (London) **586**, 702 (2020).
[31] X. Wan, A. M. Turner, A. Vishwanath, and S. Y. Savrasov, Topological semimetal and Fermi-arc surface states in the electronic structure of pyrochlore iridates, Phys. Rev. B **83**, 205101 (2011).
[32] S. M. Young, S. Zaheer, J. C. Y. Teo, C. L. Kane, E. J. Mele, and A. M. Rappe, Dirac Semimetal in Three Dimensions, Phys. Rev. Lett. **108**, 140405 (2012).
[33] Z. Wang, Y. Sun, X. Q. Chen, C. Franchini, G. Xu, H. Weng, X. Dai, and Z. Fang, Dirac semimetal and topological phase transitions in A_3 Bi (A = Na, K, Rb), Phys. Rev. B **85**, 195320 (2012).
[34] Z. K. Liu, J. Jiang, B. Zhou, Z. J. Wang, Y. Zhang, H. M. Weng, D. Prabhakaran, S. K. Mo, H. Peng, P. Dudin, T. Kim, M. Hoesch, Z. Fang, X. Dai, Z. X. Shen, D. L. Feng, Z. Hussain, and Y. L. Chen, A stable three-dimensional topological Dirac semimetal Cd_3 As_2, Nat. Mater. **13**, 677 (2014).

[35] B. J. Yang and N. Nagaosa, Classification of stable three-dimensional Dirac semimetals with nontrivial topology, Nat. Commun. **5**, 4898 (2014).

[36] J. L. Mañes, Existence of bulk chiral fermions and crystal symmetry, Phys. Rev. B **85**, 155118 (2012).

[37] T. Bzdušek, Q. S. Wu, A. Rüegg, M. Sigrist, and A. A. Soluyanov, Nodal-chain metals, Nature (London) **538**, 75 (2016).

[38] J. Yang, C. Fang, and Z. X. Liu, Symmetry-protected nodal points and nodal lines in magnetic materials, Phys. Rev. B **103**, 245141 (2021).

[39] A. A. Burkov, M. D. Hook, and L. Balents, Topological nodal semimetals, Phys. Rev. B **84**, 235126 (2011).

[40] R. Yu, H. Weng, Z. Fang, X. Dai, and X. Hu, Topological Node-Line Semimetal and Dirac Semimetal State in Antiperovskite Cu_3 PdN, Phys. Rev. Lett. **115**, 036807 (2015).

[41] Y. Kim, B. J. Wieder, C. L. Kane, and A. M. Rappe, Dirac Line Nodes in Inversion-Symmetric Crystals, Phys. Rev. Lett. **115**, 036806 (2015).

[42] B. Bradlyn, J. Cano, Z. Wang, M. G. Vergniory, C. Felser, R. J. Cava, and B. A. Bernevig, Beyond Dirac and Weyl fermions: Unconventional quasiparticles in conventional crystals, Science **353**, aaf5037 (2016).

[43] J. Cano, B. Bradlyn, and M. G. Vergniory, Multifold nodal points in magnetic materials, APL Mater. **7**, 101125 (2019).

[44] Y. Du, F. Tang, D. Wang, L. Sheng, E. J. Kan, C. G. Duan, S. Y. Savrasov, and X. Wan, CaTe: A new topological node-line and Dirac semimetal, npj Quant. Mater. **2**, 3 (2017).

[45] F. Tang and X. Wan, Effective models for nearly ideal Dirac semimetals, Front. Phys. **14**, 43603 (2019).

[46] L. Wu, F. Tang, and X. Wan, Symmetry-enforced band nodes in 230 space groups, Phys. Rev. B **104**, 045107 (2021).

[47] F. Tang and X. Wan, Exhaustive construction of effective models in 1651 magnetic space groups, Phys. Rev. B **104**, 085137 (2021).

[48] F. Tang, H. C. Po, A. Vishwanath, and X. Wan, Topological materials discovery by large-order symmetry indicators, Sci. Adv. **5**, eaau8725 (2019).

[49] F. Tang, H. C. Po, A. Vishwanath, and X. Wan, Efficient topological materials discovery using symmetry indicators, Nat. Phys. **15**, 470 (2019).

[50] G. Xu, H. Weng, Z. Wang, X. Dai, and Z. Fang, Chern Semimetal and the Quantized Anomalous Hall Effect in $HgCr_2Se_4$, Phys. Rev. Lett. **107**, 186806 (2011).

[51] J. Kruthoff, J. de Boer, J. van Wezel, C. L. Kane, and R. J. Slager, Topological Classification of Crystalline Insulators Through Band Structure Combinatorics, Phys. Rev. X **7**, 041069 (2017).

[52] J. Zhang, Y. H. Chan, C. K. Chiu, M. G. Vergniory, L. M. Schoop, and A. P. Schnyder, Topological band crossings in hexagonal materials, Phys. Rev. Mater. **2**, 074201 (2018).

[53] Y. H. Chan, B. Kilic, M. M. Hirschmann, C. K. Chiu, L. M. Schoop, D. G. Joshi, and A. P. Schnyder, Symmetry-enforced band crossings in trigonal materials: Accordion states and Weyl nodal lines, Phys. Rev. Mater. **3**, 124204 (2019).

[54] A. Leonhardt, M. M. Hirschmann, N. Heinsdorf, X. Wu, D. H. Fabini, and A. P. Schnyder, Symmetry-enforced topological band crossings in orthorhombic crystals: Classification and materials discovery, Phys. Rev. Mater. **5**, 124202 (2021).

[55] R. J. Slager, A. Mesaros, and V. Juričić, The space group classification of topological band-insulators, Nat. Phys. **9**, 98 (2013).

[56] F. Tang and X. Wan, Complete classification of band nodal structures and massless excitations, Phys. Rev. B **105**, 155156 (2022).

[57] W. Chen, H. Z. Lu, and J. M. Hou, Topological semimetals with a double-helix nodal link, Phys. Rev. B **96**, 041102(R) (2017).

[58] Z. Yan, R. Bi, H. Shen, L. Lu, S. C. Zhang, and Z. Wang, Nodal-link semimetals, Phys. Rev. B **96**, 041103(R) (2017).

[59] M. Ezawa, Topological semimetals carrying arbitrary Hopf numbers: Fermi surface topologies of a Hopf link, Solomon's knot, trefoil knot, and other linked nodal varieties, Phys. Rev. B **96**, 041202(R) (2017).

[60] P. Y. Chang and C. H. Yee, Weyl-link semimetals, Phys. Rev. B **96**, 081114(R) (2017).

[61] Z. M. Yu, Z. Zhang, G. B. Liu, W. Wu, X. P. Li, R. W. Zhang, S. A. Yang, and Y. Yao, Encyclopedia of emergent particles in three-dimensional crystals, Sci. Bull. **67**, 375 (2022).

[62] W. Wu, Y. Liu, S. Li, C. Zhong, Z. M. Yu, X. L. Sheng, Y. X. Zhao, and S. A. Yang, Nodal surface semimetals: Theory and material realization, Phys. Rev. B **97**, 115125 (2018).

[63] W. Wu, Z. M. Yu, X. Zhou, Y. X. Zhao, and S. A. Yang, Higher-order Dirac fermions in three dimensions, Phys. Rev. B **101**, 205134 (2020).

[64] G. B. Liu, Z. Zhang, Z. M. Yu, S. A. Yang, and Y. Yao, Systematic investigation of emergent particles in type-III magnetic space groups, Phys. Rev. B **105**, 085117 (2022).

[65] Z. Zhang, G. B. Liu, Z. M. Yu, S. A. Yang, and Y. Yao, Encyclopedia of emergent particles in type-IV magnetic space groups, Phys. Rev. B **105**, 104426 (2022).

[66] H. Watanabe, H. C. Po, M. P. Zaletel, and A. Vishwanath, Filling-Enforced Gaplessness in Band Structures of the 230 Space Groups, Phys. Rev. Lett. **117**, 096404 (2016).

[67] S. M. Young and B. J. Wieder, Filling-Enforced Magnetic Dirac Semimetals in Two Dimensions, Phys. Rev. Lett. **118**, 186401 (2017).

[68] R. Chen, H. C. Po, J. B. Neaton, and A. Vishwanath, Topological materials discovery using electron filling constraints, Nat. Phys. **14**, 55 (2018).

[69] D. Wang, F. Tang, H. C. Po, A. Vishwanath, and X. Wan, XFe_4 Ge_2 X=Y, Lu) and Mn_3 Pt: Filling-enforced magnetic topological metals, Phys. Rev. B **101**, 115122 (2020).

[70] S. Ono and K. Shiozaki, Symmetry-Based Approach to Superconducting Nodes: Unification of Compatibility Conditions and Gapless Point Classifications, Phys. Rev. X **12**, 011021 (2022).

[71] F. Tang, S. Ono, X. Wan, and H. Watanabe, High-Throughput Investigations of Topological and Nodal Superconductors, Phys. Rev. Lett. **129**, 027001 (2022).

[72] Z. Wang, A. Alexandradinata, R. J. Cava, and B. A. Bernevig, Hourglass fermions, Nature (London) **532**, 189 (2016).

[73] S. S. Wang, Y. Liu, Z. M. Yu, X. L. Sheng, and S. A. Yang, Hourglass Dirac chain metal in rhenium dioxide, Nat. Commun. **8**, 1 (2017).

[74] L. Wu, F. Tang, and X. Wan, Exhaustive list of topological hourglass band crossings in 230 space groups, Phys. Rev. B **102**, 035106 (2020).

[75] Bahadur Singh, Barun Ghosh, Chenliang Su, Hsin Lin, Amit Agarwal, and Arun Bansil, Topological Hourglass Dirac Semimetal in the Nonpolar Phase of Ag_2BiO_3, Phys. Rev. Lett. **121**, 226401 (2018).

[76] B. Fu, X. Fan, D. Ma, C.-C. Liu, and Y. Yao, Hourglasslike nodal net semimetal in Ag_2BiO_3, Phys. Rev. B **98**, 075146 (2018).

[77] Z. Guguchia, J. A. T. Verezhak, D. J. Gawryluk, S. S. Tsirkin, J.-X. Yin, I. Belopolski, H. Zhou, G. Simutis, S.-S. Zhang, T. A. Cochran, G. Chang, E. Pomjakushina, L. Keller, Z. Skrzeczkowska, Q. Wang, H. C. Lei, R. Khasanov, A. Amato, T. Neupert S. Jia, H. Luetkens *et al.*, Tunable anomalous Hall conductivity through volume-wise magnetic competition in a topological kagome magnet, Nat. Commun. **11**, 559 (2020).

[78] E. Cheng, W. Xia, X. Shi, H. Fang, C. Wang, C. Xi, S. Xu, D. C. P., L. Wang, H. Su, L. Pi, W. Ren, X. Wang, N. Yu, Y. Chen, W. Zhao, Z. Liu, Y. Guo, and S. Li, Magnetism-induced topological transition in $EuAs_3$, Nat. Commun. **12**, 6970 (2021).

[79] Y. Jin, X. T. Zeng, X. Feng, X. Du, W. Wu, X. L. Sheng, Z. M. Yu, Z. Zhu, and S. A. Yang, Multiple magnetism-controlled topological states in EuAgAs, Phys. Rev. B **104**, 165424 (2021).

[80] A. H. Mayo, H. Takahashi, M. S. Bahramy, A. Nomoto, H. Sakai, and S. Ishiwata, Magnetic Generation and Switching of Topological Quantum Phases in a Trivial Semimetal α-EuP_3, Phys. Rev. X **12**, 011033 (2022).

[81] D. Wang, F. Tang, J. Ji, W. Zhang, A. Vishwanath, H. C. Po, and X. Wan, Two-dimensional topological materials discovery by symmetry-indicator method, Phys. Rev. B **100**, 195108 (2019).

[82] See the Supplemental Material I at http://link.aps.org/supplemental/10.1103/PhysRevB.106.165128 for all the detailed results on magnetic layer (space) groups for essential and nonessential hourglass fermions, which includes Refs. [47,74,87].

[83] S. V. Gallego, J. M. Perez-Mato, L. Elcoro, E. S. Tasci, R. M. Hanson, M. I. A. K. Momma, and G. Madariaga, MAGNDATA: Toward a database of magnetic structures. I. The commensurate case, J. Appl. Crystallogr. **49**, 1750 (2016).

[84] http://webbdcrista1.ehu.es/magndata/.

[85] See the Supplemental Material II at http://link.aps.org/supplemental/10.1103/PhysRevB.106.165128 for the calculated magnetic moments and band structures of 175 magnetic hourglass materials, which includes Refs. [83,88].

[86] N. V. Belov, N. N. Neronova, and T. S. Smirnova, Shubnikov groups, Sov. Phys. Crystallogr. **2**, 311 (1957).

[87] C. J. Bradley and A. P. Cracknell, *The Mathematical Theory of Symmetry in Solids* (Oxford University press, Oxford, 1972).

[88] V. I. Anisimov, F. Aryasetiawan, and A. I. Lichtenstein, First-principles calculations of the electronic structure and spectra of strongly correlated systems: the LDA + U method, J. Phys.: Condens. Matter **9**, 767 (1997).

[89] V. V. Klepov, K. A. Pace, A. A. Berseneva, J. B. Felder, S. Calder, G. Morrison, Q. Zhang, M. J. Kirkham, D. S. Parker, and H. C. zurLoye, Chloride reduction of Mn^{3+} in mild hydrothermal synthesis of a charge ordered defect pyrochlore, $CsMn^{2+}\ Mn^{3+}\ F_6$, a canted antiferromagnet with a hard ferromagnetic component, J. Am. Chem. Soc. **143**, 11554 (2021).

[90] V. N. Nguyen, F. Tchéou, and J. Rossat-Mignod, Magnetic structures of PrSi and NdSi intermetallic alloys, Solid State Commun. **23**, 821 (1977).

[91] K. S. V. L. Narasimhan and H. Steinfink, Magnetic investigations on AlB2 type structures, J. Solid State Chem. **10**, 137 (1974).

[92] Q. M. Zhang, L. Gao, L. Cui, L. C. Wang, C. L. Fu, Z. Y. Xu, Z. J. Mo, W. Cai, G. Chen, and X. L. Deng, Magnetic properties and magnetocaloric effect of the compound NdSi, Phys. B: Condens. Matter **456**, 258 (2015).

[93] X. Miao, Y. Gong, L. Caron, Y. You, G. Xu, D. Sheptyakov, P. Manuel, F. Qian, Y. Zhang, F. Xu, N. van Dijk, and E. Brück, Switching the magnetostructural coupling in MnCoGe-based magnetocaloric materials, Phys. Rev. Mater. **4**, 104407 (2020).

[94] Y. Y. Zhao, F. X. Hu, L. F. Bao, J. Wang, H. Wu, Q. Z. Huang, R. R. Wu, Y. Liu, F. R. Shen, H. Kuang, M. Zhang, W. L. Zuo, X. Q. Zheng, J. R. Sun, and B. G. Shen, Giant negative thermal expansion in bonded MnCoGe-based compounds with Ni_2In-type hexagonal structure, J. Am. Chem. Soc. **137**, 1746 (2015).

[95] G. J. Li, E. K. Liu, H. G. Zhang, Y. J. Zhang, J. L. Chen, W. H. Wang, H. W. Zhang, G. H. Wu, and S. Y. Yu, Phase diagram, ferromagnetic martensitic transformation and magnetoresponsive properties of Fe-doped MnCoGe alloys, J. Magn. Magn. Mater. **332**, 146 (2013).

[96] F. Fei, X. Bo, R. Wang, B. Wu, J. Jiang, D. Fu, M. Gao, H. Zheng, Y. Chen, X. Wang, H. Bu, F. Song, X. Wan, B. Wang, and G. Wang, Nontrivial Berry phase and type-II Dirac transport in the layered material $PdTe_2$, Phys. Rev. B **96**, 041201(R) (2017).

[97] H. J. Noh, J. Jeong, E. J. Cho, K. Kim, B. I. Min, and B. G. Park, Experimental Realization of Type-II Dirac Fermions in a $PdTe_2$ Superconductor, Phys. Rev. Lett. **119**, 016401 (2017).

[98] M. Yan, H. Huang, K. Zhang, E. Wang, W. Yao, K. Deng, G. Wan, H. Zhang, Masashi Arita, H. Yang, Z. Sun, H. Yao, Y. Wu, S. Fan, W. Duan, and S. Zhou, Lorentz-violating type-II Dirac fermions in transition metal dichalcogenide $PtTe_2$, Nat. Commun. **8**, 257 (2017).

[99] K. Zhang, M. Yan, H. Zhang, H. Huang, M. Arita, Z. Sun, W. Duan, Y. Wu, and S. Zhou, Experimental evidence for type-II Dirac semimetal in $PtSe_2$, Phys. Rev. B **96**, 125102 (2017).

[100] G. Pizzi, V. Vitale, R. Arita, S. Blügel, F. Freimuth, G. Géranton, M. Gibertini, D. Gresch, C. Johnson, T. Koretsune, J. Ibañez-Azpiroz, H. Lee, J. M. Lihm, D. Marchand, A. Marrazzo, Y. Mokrousov, J. I. Mustafa, Y. Nohara, Y. Nomura, L. Paulatto *et al.*, Wannier90 as a community code: New features and applications, J. Phys.: Condens. Matter **32**, 165902 (2020).

[101] A. A. Mostofi, J. R. Yates, Y. S. Lee, I. Souza, D. Vanderbilt, and N. Marzari, Wannier90: A tool for obtaining maximally localized Wannier functions, Comput. Phys. Commun. **178**, 685 (2008).

[102] N. Marzari and D. Vanderbilt, Maximally localized generalized Wannier functions for composite energy bands, Phys. Rev. B **56**, 12847 (1997).

[103] I. Souza, N. Marzari, and D. Vanderbilt, Maximally localized Wannier functions for entangled energy bands, Phys. Rev. B **65**, 035109 (2001).